ACADEMIC PRESS

Available online at www.sciencedirect.com

SCIENCE DIRECT®

Atomic Data and Nuclear Data Tables 83 (2003) 45–69

Atomic Data AND Nuclear Data Tables

www.elsevier.com/locate/adt

Scattering angle-integrated (total) and magnetic sublevel cross-sections and degree of linear polarization for electron and proton induced excitation [HeI (1snp) $^1P^0$ ($n = 2$–5)] of helium☆

H. Merabet,[a,*] R. Bruch,[a] J. Hanni,[a] M. Bailey,[a] A.L. Godunov,[b] J.H. McGuire,[b] D.V. Fursa,[c] I. Bray,[c] K. Bartschat,[d] H.C. Tseng,[e] and C.-D. Lin[f]

[a] *Department of Physics, University of Nevada, Reno, NV 89557, USA*
[b] *Department of Physics, Tulane University, New Orleans, LA 70118, USA*
[c] *Centre for Atomic, Molecular and Surface Physics, School of Mathematical and Physical Sciences, Murdoch University, Perth 6150, Australia*
[d] *Department of Physics and Astronomy, Drake University, Des Moines, IA 50311, USA*
[e] *Department of Physics, Chung Yuan Christian University, Chung Li 32023, Taiwan*
[f] *Department of Physics, Kansas State University, Manhattan, KS 66506, USA*

Abstract

Experimental scattering-angle-integrated (total) cross-sections $\bar{\sigma}$, (scattering) angle-integrated magnetic sublevel cross-sections $\bar{\sigma}_{M_L}$, and degree of linear polarization data have been measured in the extreme ultraviolet (EUV) wavelength region following decay of HeI (1snp) $^1P^0$ ($n = 2$–5) states induced by electron and proton impact on a neutral helium target. These measurements are compared with a first Born approach as well as more sophisticated theoretical calculations. Specifically, theoretical values for electron impact include convergent close-coupling (CCC) and *R*-matrix with pseudo states (RMPS) methods in addition to first Born (Born 1) approximation while proton induced excitation cross-sections are compared with atomic-orbital close-coupling (AOCC) and first Born predictions.

☆ Data files associated with this article may be found on ScienceDirect at http://www.sciencedirect.com.

* Corresponding author. Fax: 1-775-784-1398.
E-mail address: hocine@physics.unr.edu (H. Merabet).

0092-640X/03/$ - see front matter © 2003 Elsevier Science (USA). All rights reserved.
doi:10.1016/S0092-640X(02)00017-7

Contents

1. Introduction

Helium is the second most abundant element in the universe with numerous academic, industrial and astrophysical applications. For example, radiative emissions from singly charged ions like He^+ have been observed in solar spectra under solar-flare conditions [1]. The study of such complex non-equilibrium, anisotropic, beam-like systems may provide a deeper comprehension of induced proton jets in solar flare astrophysical investigations. Furthermore, radiative emissions from neutral and ionized helium play a major role in laboratory plasmas driven by high intensity, ultrafast femtosecond laser interactions with gases and solid surfaces [2]. The plasma created is in many cases anisotropic with non-Maxwellian electron distributions leading to bright, ultrafast X-ray production [2,3].

Although angle-differential measurements and calculations for electron-impact excitation have been reported [4–8], many investigations of the cross-sections by proton and electron impact have concentrated on scattering-angle-integrated (total) cross-sections, obtained by observing the radiation emitted in the subsequent optical decay of the excited states. Such studies have been limited due to the complications arising from cascade re-population of studied states, effects caused by polarization which relates to the observed emission cross-sections, and the difficulty in finding an absolute calibration of the cross-sections obtained with many experimental setups [9]. The only measured sublevel cross-sections for the helium excitation are those obtained with a procedure, where the ratio of the magnetic sublevel (scattering) angle-differential cross-section, σ_0, to the differential cross-section, called the parameter $\lambda = \sigma_0/(\sigma_0 + 2\sigma_1)$, is determined experimentally using electron-photon coincidence techniques [10]. The λ parameter, combined with available double differential cross-section ($\sigma = \sigma_0 + 2\sigma_1$) data, yields σ_0. This ap-

proach has been utilized by Chutjian et al. [11] for the excitation of the HeI (1s2p) $^1P^0$ level, at 60 and 80 eV electron impact energies, and the HeI (1s3p) $^1P^0$ level at 80 and 100 eV [12]; whereas Hummer et al. [13] have directly obtained the relative σ_0 for the excitation of the HeI (1s3p) $^1P^0$ state at 70 eV as a function of the scattering angle. Furthermore, Harris [14] have measured triple differential cross-sections for HeI (1s3p) $^1P^0$ for an electron impact energy of 40 eV. In addition, Csanak et al. [15] have used the λ parameter procedure to extract HeI (1snp) $^1P^0$ ($n = 2$–3) triply differential cross-sections and have computed the corresponding theoretical integral values for $n = 2$–6 with incident energy in the 25–500 eV range, using first-order many-body theory (FOMBT) [16]. To our knowledge, no experimental data are available for the HeI (1snp) $^1P^0$ $n \geqslant 4$ levels.

In the present paper we provide, in addition to total cross-sections over a wide range of projectile energies, the scattering-angle-integrated magnetic sublevel cross-sections, their ratios as well as the degree of linear polarization and the alignment parameters associated with the excited states HeI (1snp) $^1P^0$ ($n = 2$–5) for projectile velocities ranging from 2 to 10 a.u. Moreover, we have compiled here a comprehensive experimental and theoretical database for single excitation of helium following electron and proton impact using extreme ultraviolet (EUV) spectropolarimetry techniques [17–21] and advanced theoretical procedures, namely the convergent close-coupling (CCC) [22,23], *R*-matrix with pseudo-states (RMPS) [24,25] and atomic-orbital close-coupling (AOCC) [26] methods. The processes investigated in this study are:

$$\begin{aligned} A + \mathrm{He} \rightarrow \quad & \mathrm{He}\ (1snp)\ {}^1P^0 + A \\ & \downarrow \\ & \mathrm{He}\ (1s^2)\ {}^1S + h\nu, \end{aligned} \tag{1}$$

where A is e^- or H^+ and the emitted EUV radiation is observed at 90° with respect to the projectile beam. In our experiment, we have utilized a cylindrically symmetric collision geometry, hence the degree of linear polarization P can be defined as

$$P = \frac{I_\parallel - I_\perp}{I_\parallel + I_\perp}. \tag{2}$$

Here $I_\parallel$ and $I_\perp$ are the intensities of radiation with electric field vectors parallel and perpendicular with respect to the incident projectile beam direction when measured at an angle of 90°. P is directly related to the sublevel cross-section ratios. Assuming LS-coupling, where L and S are the orbital and spin angular momentum numbers of the excited levels, P, for HeI (1snp) $^1P^0$ states, can be expressed as [17]

$$P\ (^1P^0) = \frac{\bar\sigma_0 - \bar\sigma_1}{\bar\sigma_0 + \bar\sigma_1} = \frac{r-1}{r+1}, \tag{3}$$

where $\bar\sigma_{M_L}$ ($M_L = -1, 0$, and 1) are the magnetic sublevel excitation cross-sections of specific M_L substates and $r = \bar\sigma_0/\bar\sigma_1$, is the cross-section ratio. Moreover, the total cross-section $\bar\sigma$ is the sum of the three magnetic sublevel cross-sections,

$$\bar\sigma = \bar\sigma_0 + 2\bar\sigma_1. \tag{4}$$

Thus by combining Eq. (3) with Eq. (4), $\bar\sigma_{M_L}$ can be obtained for the excitation process.

1.1. Experimental setup and cross-sections determination

The experimental setup used in this work consists of three main components: an EUV polarimeter; an electron gun or a 2 MV Van de Graaff accelerator, target cell and Faraday cup; and a 1.5 m grazing incidence monochromator. A PC controlled data acquisition system has been used to operate the apparatus and to record the data. A detailed description of this experimental setup is given by Bailey et al. [20,27,28]. In brief, the polarimeter utilizes a molybdenum–silicon (Mo/Si) MLM whose surface reflection has been used for radiation with wavelengths $\lambda \approx 584$ Å at an incidence angle of 40° corresponding to the HeI (1snp) $^1P^0 \rightarrow (1s^2)\ ^1S$ ($n = 2$–5) transitions. It is assumed here that the degree of linear polarization does not depend on the principal quantum number n [19]. The corresponding total cross-sections $\bar\sigma$ measurements have been conducted using a 1.5 m high resolution grazing incidence monochromator [17,27]. These results have been put on an absolute scale by normalizing our data to the Bethe–Born cross-section values [29], for electron and proton impact, at high velocities. This normalization procedure has been described in more details in [27]. In this work, the cross-section data obtained have also been improved[1] for alignment effects using [30],

$$\bar\sigma(\theta) = \bar\sigma \times \{1 + A_0 P_2(\cos\theta)\}, \tag{5}$$

where $\bar\sigma(\theta)$ is the measured cross-section, $\theta = 90°$ is the observation angle of the emitted photons, $\bar\sigma$ is the cross-section for an isotropic distribution, $P_2(\cos\theta)$ is the second Legendre polynomial, and A_0 (see GRAPH II, Figure 8) is the alignment parameter related to the degree of linear polarization by

$$P(^1P^0) = \frac{3A_0}{A_0 - 2}. \tag{6}$$

Statistics of the measured line intensities can introduce additional uncertainties ranging from approximately 1% for HeI (1s2p) $^1P^0$ up to 8% for HeI (1s5p) $^1P^0$ decays. When instrumental uncertainties related to energy resolution of the Van de Graaff accelerator, target pressure stability, polarization, and charge

[1] The cross-section corrections due to alignment effects have been found to be between 1% and 5%.

normalization are combined, total experimental uncertainties for differential cross-sections ranging from 8% for HeI (1s2p) to 18% for HeI (1s5p) are obtained. The corresponding total uncertainty for magnetic scattering angle-integrated substate cross-sections are found to be about 10%–13% for HeI (1s2p) and HeI (1s3p) and about 17%–24% for the higher levels HeI (1snp) with $n = 4$–5 (see TABLES).

1.2. Calculation methods

In the present section we give very short descriptions of different theoretical calculations used to compile magnetic scattering angle-integrated substate cross-sections, polarization fractions, and total cross-sections for the HeI (1snp) $^1P^0$ states. Further details of these methods are given elsewhere [22–26].

1.2.1. Convergent close-coupling calculations for $e^- + He$ collisions

The details of the CCC method for e–He scattering are found in [22]. Briefly, the total wavefunction is expanded using a set of two-electron states obtained by diagonalizing the target Hamiltonian in an explicitly antisymmetric basis of Laguerre functions. In this work, the frozen-core approximation is employed where for all states one of the orbitals is the ground state 1s of He^+ with the other orbital being a linear combination of Laguerre functions. The strength of this approximation is that the excited states are described quite accurately. The disadvantage of this method is that the ground state is not very precisely defined. Relaxing the frozen-core approximation would lead to the generation of too numerous states to solve the subsequent coupled equations on our presently available computers. However, we may do so if we approximate the solution of the coupled equations by the unitary, Born, or the distorted-wave Born approximation. Thus, we are readily able to test the frozen-core approximation at the higher energies where the above approximations yield sufficiently accurate results. The frozen-core model was used and checked at the higher energies by comparison with the Born approximation with and without the frozen-core model. It was found that once the Born approximation, using the frozen-core model target structure agrees with the CCC results, the Born approximation with substantially improved target states reduces these by approximately 10%.

1.2.2. R-matrix calculations for $e^- + He$ collisions

The RMPS calculation performed for $e^- + He$ collisions in the present study is an extension of the work described by Bartschat et al. [24] to higher energies. This extension was achieved by increasing the number of continuum orbitals, which are used to expand the wavefunction of the continuum electron inside the R-matrix box from 27 to 50. It thus allowed for the calculation of converged results for the HeI $(1s^2)\ ^1S \rightarrow (1s2p)\ ^1P^0$ transition up to incident energies of 400 eV. As in the CCC-model described above, the physical states (we only used the five lowest states of helium) were supplemented by a number of pseudo-states (36 in this case) to represent the channel coupling to the higher-lying discrete states as well as the continuum states of the target. The RMPS model yielded an excellent (relative to most other collision calculations) description of the target for both the relevant energy levels and oscillator strengths. Hence, the RMPS results are expected to be reliable, for the allowed transitions studied here, over the entire energy region for which they were calculated, with the exception of resonances in the narrow window of incident energies between the physical states with $n > 2$ and the ionization threshold. In particular, we note that the RMPS results are expected to converge toward first-Born predictions obtained with equally sophisticated target descriptions.

1.2.3. Atomic-orbital close-coupling calculations for $H^+ + He$ collisions

For $H^+ + He$ collisions the excitation cross-sections and polarization fractions for He (1snp) $^1P^0$ states are calculated using the standard close-coupling expansion method. By treating the Schrödinger equation for the two electrons in the Coulomb fields of the two moving nuclei, we expanded the time-dependent wavefunction in terms of the eigenstates of He. In the energy region under study, charge transfer processes are not important such that the basis functions included are all centered around the target atom. In other words only the helium eigenstates are used in the expansion. Following the standard procedure, the resulting expansion coefficients satisfy a system of linear first-order differential equations for each collision impact parameter. The excitation cross-section to each magnetic substate is calculated by integrating the excitation probability over the impact parameter plane. Details of such calculations can be found in the review by Fritsch and Lin [26]. In this calculation, basis states consist of singly excited states up to $n = 3$ and some pseudostates for each total angular momentum L.

1.3. Results

Using Eqs. (3) and (4), we have derived experimental $\bar{\sigma}_M$ following HeI $(1snp)\ ^1P^0 \rightarrow (1s^2)\ ^1S$, $(n = 2$–$5)$, transitions at impact energies ranging from 30 to 980 eV ($1.4 < v < 8.5$ a.u.) in $e^- + He$ collisions and from 50 to 1400 keV ($1.4 < v < 7.5$ a.u.) in $H^+ + He$ collisions. For electron impact, we have used our polarization and differential cross-section data for $v \geqslant 3$ a.u., whereas at lower velocities, magnetic scattering angle-integrated substate cross-sections $\bar{\sigma}_M$ have been extracted by

combining the differential cross-sections of Westerveld et al. [5] and Donaldson et al. [6] with our polarization results for HeI (1snp) $^1P^0$ for $n = 2$–3 and $n = 4$–5, respectively.

In the following tables and figures, we present the complete set of our experimental and theoretical total, magnetic scattering angle-integrated substate cross-sections, degree of linear polarization, magnetic cross-section ratios, and alignment parameters for the HeI (1snp) $^1P^0$ ($n = 2$–5) substates.

Acknowledgments

We would like to thank Dr. Stephan Fülling for his assistance in keeping the Van de Graaff accelerator operational. This work was supported, in part, by the National Science Foundation (acknowledged by K.B.), the Nevada Business and Science Foundation and ACSPECT Corporation, Reno Nevada.

References

[1] S.A. Kazantsev, N.M. Firstova, A.V. Bulatov, A.G. Petrashen, J.-C. Henoux, Opt. Spectrosc. 78 (1995) 729.
[2] A.S. Shlyptseva, R. Mancini, JQSRT 58 (4–6) (1997) 917.
[3] R. Mancini, C.F. Hooper Jr., N.D. Delamater, A. Hauer, C.J. Keane, B.A. Hammel, J.K. Nash, Rev. Sci. Instrum. 63 (10) (1992) 5119.
[4] R. Hippler, K.H. Schartner, J. Phys. B 7 (1974) 618.
[5] W.B. Westerveld, H.G.M. Heideman, J. van Eck, J. Phys. B 12 (1979) 115.
[6] F.G. Donaldson, M.A. Hender, J.W. McConkey, J. Phys. B 5 (1972) 1192.
[7] K. Bartschat, J. Phys. B 31 (1998) L469.
[8] I.L. Beigman et al., At. Data Nucl. Data Tables 74 (2000) 123.
[9] Marchalant et al., J. Phys. B 31 (1998) 1141, and references therein.
[10] K. Blum et al., Adv. At. Mol. Phys. 19 (1983) 187.
[11] A. Chutjian et al., J. Phys. B 8 (1975) 2360.
[12] A. Chutjian, J. Phys. B 9 (1976) 1749.
[13] C.R. Hummer et al., Phys. Rev. A 33 (1986) 2995.
[14] C.L. Harris, Ph.D. Thesis, University of Nevada, Reno, 2000 (unpublished).
[15] G. Csanak et al., Phys. Rev. A 45 (1992) 1625.
[16] G. Csanak et al., Phys. Rev. A 3 (1971) 1322.
[17] H. Merabet, M. Bailey, R. Bruch, J. Hanni, S. Bliman, D.V. Fursa, I. Bray, K. Bartschat, H.C. Tseng, C.D. Lin, Phys. Rev. A 64 (2001) 012712.
[18] W. Stolte, R. Bruch, Phys. Rev. A 54 (1996) 2116.
[19] H. Merabet, M. Bailey, R. Bruch, D.V. Fursa, I. Bray, J.W. McConkey, P. Hammond, Phys. Rev. A 60 (1999) 1187.
[20] M. Bailey, H. Merabet, R. Bruch, Appl. Opt. 38 (19) (1999) 4125.
[21] H. Merabet, A. Siems, J. Hanni, R. Bruch, S. Fülling, M. Bailey, Proc. SPIE 4139 (2000) 80.
[22] D.V. Fursa, I. Bray, Phys. Rev. A 52 (1995) 1279.
[23] D.V. Fursa, I. Bray, J. Phys. B 30 (1997) 757.
[24] K. Bartschat, E.T. Hudson, M.P. Scott, P.G. Burke, V.M. Burke, J. Phys. B 29 (1996) 2875.
[25] E.T. Hudson, K. Bartschat, M.P. Scott, P.G. Burke, V.M. Burke, J. Phys. B 29 (1996) 5513.
[26] W. Fritsch,, C.D. Lin, Phys. Rep. 201 (1991) 1.
[27] M. Bailey, R. Bruch, E. Rauscher, S. Bliman, J. Phys. B 28 (1995) 2655.
[28] M. Bailey, M.S. Thesis, University of Nevada, Reno, 1992 (unpublished).
[29] Y.-K. Kim, M. Inokuti, Phys. Rev. 184 (1969) 38.
[30] A. Götz, W. Mehlhorn, A. Raeker, K. Bartschat, J. Phys. B 29 (1996) 4699.

Explanation of Tables

Table 1. Magnetic sublevel angle-integrated and total cross-sections for decay of He (1snp) $^1P^0$ ($n = 2$–5) states following electron and proton impact.

For projectile velocities $v < 3.8$ a.u., differential cross-sections from Westerveld et al. [5] were used for HeI (1snp) $^1P^0$ ($n = 2$–3) states. For the $n = 4$ states, cross-sections for those projectile energies were measured by Donaldson et al. [6]. The data for the $n = 5$ states were scaled from Donaldson's data using the $1/n^3$ scaling law. Magnetic scattering angle integrated substate cross-sections for those data were derived by combining them with the polarization data of Merabet et al. [19].

A. Electron cross-sections: experiment
B. Electron cross-sections: CCC
C. Electron cross-sections: Born 1
D. Electron cross-sections: RMPS
E. Proton cross-sections: experiment
F. Proton cross-sections: AOCC
G. Proton cross-sections: Born 1

Table 2. Degree of linear polarization and cross-section ratio $\bar{\sigma}_0/\bar{\sigma}_1$ for decay of HeI (1s2p) $^1P^0$ states following electron and proton impact.

Experimental polarization values for 50, 100, and 1400 keV protons were extrapolated using a least squares fit.

A. Electron data
B. Proton data

Explanation of Graphs

Graph 1. Magnetic sublevel angle-integrated and total cross-sections for decay of HeI (1snp) $^1P^0$ ($n = 2$–5) states following electron and proton induced excitation.

Figures 1–3. Electron impact cross-sections. Experiment: solid triangles, this work; open triangles, Westerveld et al. [5] ($n = 2, 3$) and Donaldson et al. [6] ($n = 4$–5). (*Note*. differential cross-sections were used from Westerveld and Donaldson's groups, but magnetic scattering angle-integrated substate cross-sections for those projectile energies were derived in combination with the polarization data of Merabet et al. [19].) Theory: dashed curve, Born 1, this work; dotted curve, RMPS, this work; solid curve, CCC, this work.

Figures 4–6. Proton impact cross-sections. Experiment: solid circles. Theory: dotted curve, Born 1, chain curve, AOCC.

Graph 2. Degree of linear polarization, alignment, and cross-section ratio $\bar{\sigma}_0/\bar{\sigma}_1$ for decay of HeI (1s2p) $^1P^0$.

Figure 7. Degree of linear polarization. Experiment: solid triangles, electrons, this work; solid circles, protons, this work. Theory: solid curve, electrons, CCC, this work; dashed curve, electrons, Born 1, this work; dotted curve, electrons, RMPS, this work; – • •–, protons, Born 1, this work; – • –, protons, AOCC, this work.

Figure 8. Alignment parameter A_0. Solid triangles, electrons; solid circles, protons. Dashed lines have been provided to guide the eye.

Figure 9. Cross-section ratio. Experiment: solid triangles, electrons, this work; solid circles, protons, this work. Theory: solid curve, electrons, CCC, this work; dashed curve, electrons, Born 1, this work; dotted curve, electrons, RMPS, this work; – • •–, protons, Born 1, this work; – • –, protons, AOCC, this work.

Table 1A
Magnetic sublevel angle-integrated and total cross-sections for decay of He (1snp) $^1P^0$ ($n = 2$–5) states following electron and proton impact – A. Electron cross-sections: Experiment. See page 50 for Explanation of Tables

Energy (eV)	Velocity (a.u.)	HeI (1s2p) $^1P^0$			HeI (1s3p) $^1P^0$		
		$\bar{\sigma}_0$ (10^{-19}cm^2)	$\bar{\sigma}_1$ (10^{-19}cm^2)	$\bar{\sigma}$ (10^{-19}cm^2)	$\bar{\sigma}_0$ (10^{-19}cm^2)	$\bar{\sigma}_1$ (10^{-19}cm^2)	$\bar{\sigma}$ (10^{-19}cm^2)
30	1.5	30.3 ± 2.7	9.6 ± 0.9	49.5 ± 4.5[a]	5.6 ± 0.5	1.8 ± 0.2	9.2 ± 0.8[a]
60	2.1	64.6 ± 6.6	20.4 ± 2.1	105.4 ± 9.5[a]	14.2 ± 1.4	4.5 ± 0.5	23.2 ± 2.1[a]
80	2.4	61.4 ± 6.6	24.5 ± 2.6	110.4 ± 9.9[a]	14.3 ± 1.5	5.7 ± 0.6	25.7 ± 2.3[a]
150	3.3	43.4 ± 5.5	27.2 ± 3.4	97.8 ± 8.8[a]	10.4 ± 1.3	6.5 ± 0.8	23.5 ± 2.1[a]
200	3.8	37.4 ± 3.9	27.3 ± 2.8	92.0 ± 6.9	9.7 ± 1.0	7.1 ± 0.7	23.9 ± 1.8
276	4.5	27.6 ± 2.9	23.5 ± 2.5	74.7 ± 5.6	6.8 ± 0.7	5.8 ± 0.6	18.5 ± 1.4
340	5.0	21.7 ± 2.3	20.7 ± 2.2	63.1 ± 4.7	5.3 ± 0.6	5.1 ± 0.5	15.5 ± 1.2
412	5.5	18.6 ± 2.0	19.5 ± 2.1	57.6 ± 4.3	4.8 ± 0.5	5.0 ± 0.5	14.9 ± 1.1
500	6.1	16.2 ± 1.7	17.9 ± 1.9	51.9 ± 3.9	4.3 ± 0.5	4.8 ± 0.5	13.9 ± 1.0
575	6.5	13.6 ± 1.4	16.2 ± 1.7	45.9 ± 3.4	3.4 ± 0.4	4.1 ± 0.4	11.5 ± 0.9
667	7.0	13.3 ± 1.4	16.5 ± 1.8	46.2 ± 3.5	3.4 ± 0.4	4.2 ± 0.4	11.7 ± 0.9
735	7.3	11.2 ± 1.2	14.2 ± 1.5	39.6 ± 3.0	3.1 ± 0.3	3.9 ± 0.4	11.0 ± 0.8
836	7.8	9.6 ± 1.0	12.4 ± 1.3	34.4 ± 2.6	2.3 ± 0.3	3.0 ± 0.3	8.4 ± 0.6
980	8.5	9.4 ± 1.0	12.4 ± 1.3	34.1 ± 2.6	2.4 ± 0.3	3.2 ± 0.3	8.7 ± 0.7
		HeI (1s4p)$^1P^0$			HeI (1s5p)$^1P^0$		
30	1.5	1.9 ± 0.8	0.6 ± 0.3	3.1 ± 1.2[a]	0.97 ± 0.42	0.31 ± 0.13	1.59 ± 0.60[a]
60	2.1	5.9 ± 3.2	1.9 ± 1.0	9.6 ± 3.6[a]	3.01 ± 1.62	0.95 ± 0.51	4.92 ± 1.87[a]
80	2.4	5.9 ± 3.2	2.4 ± 1.3	10.6 ± 4.0[a]	3.02 ± 1.64	1.20 ± 0.65	5.43 ± 2.06[a]
150	3.3	4.4 ± 2.5	2.8 ± 1.5	9.9 ± 3.8[a]	1.69 ± 1.26	1.41 ± 0.79	5.07 ± 1.93[a]
200	3.8	3.9 ± 0.7	2.8 ± 0.5	9.5 ± 1.1	1.92 ± 0.42	1.40 ± 0.30	4.73 ± 0.71
276	4.5	3.0 ± 0.5	2.5 ± 0.4	8.0 ± 1.0	1.36 ± 0.30	1.16 ± 0.25	3.67 ± 0.55
340	5.0	2.1 ± 0.4	2.0 ± 0.4	6.2 ± 0.7	0.99 ± 0.22	0.95 ± 0.21	2.88 ± 0.43
412	5.5	1.9 ± 0.3	2.0 ± 0.3	5.8 ± 0.7	0.79 ± 0.17	0.82 ± 0.18	2.43 ± 0.36
500	6.1	1.7 ± 0.3	1.9 ± 0.3	5.6 ± 0.7	0.77 ± 0.17	0.85 ± 0.19	2.48 ± 0.37
575	6.5	1.6 ± 0.3	1.9 ± 0.3	5.4 ± 0.6	0.67 ± 0.15	0.80 ± 0.17	2.26 ± 0.34
667	7.0	1.2 ± 0.2	1.5 ± 0.3	4.3 ± 0.5	0.57 ± 0.13	0.71 ± 0.16	1.99 ± 0.30
735	7.3	1.1 ± 0.2	1.4 ± 0.2	3.9 ± 0.5	0.55 ± 0.12	0.70 ± 0.15	1.95 ± 0.29
836	7.8	0.84 ± 0.1	1.1 ± 0.2	3.0 ± 0.4	0.42 ± 0.09	0.54 ± 0.12	1.49 ± 0.22
980	8.5	0.91 ± 0.2	1.2 ± 0.2	3.3 ± 0.4	0.53 ± 0.12	0.70 ± 0.15	1.92 ± 0.29

[a] Experimental polarization values for 50, 100, and 1400 keV protons were extrapolated using a least squares fit.

Table 1B
Magnetic sublevel angle-integrated and total cross-sections for decay of He (1snp) $^1P^0$ ($n = 2$–5) states following electron and proton impact – B. Electron cross-sections: CCC. See page 50 for Explanation of Tables

Energy (eV)	Velocity (a.u.)	HeI (1s2p) $^1P^0$			HeI (1s3p) $^1P^0$		
		$\bar{\sigma}_0$ (10^{-19}cm^2)	$\bar{\sigma}_1$ (10^{-19}cm^2)	$\bar{\sigma}$ (10^{-19}cm^2)	$\bar{\sigma}_0$ (10^{-19}cm^2)	$\bar{\sigma}_1$ (10^{-19}cm^2)	$\bar{\sigma}$ (10^{-19}cm^2)
35	1.6	35.6	8.0	51.5	7.2	1.6	10.3
65	2.2	57.0	20.3	97.6	13.2	4.0	21.2
80	2.4	59.8	24.9	109.6	14.5	5.6	25.6
150	3.3	45.1	28.8	102.6	12.2	6.9	26.1
200	3.8	36.6	27.5	91.6	9.1	6.7	22.5
276	4.5	28.4	25.2	78.7	7.1	6.2	19.4
340	5.0	23.8	23.2	70.2	5.9	5.7	17.4
412	5.5	20.1	21.3	62.7	5.0	5.3	15.5
500	6.1	16.8	19.4	55.5	4.2	4.8	13.8
575	6.5	14.8	18.0	50.7	3.7	4.4	12.6
667	7.0	12.9	16.5	45.9	3.2	4.1	11.4
735	7.3	11.7	15.6	42.9	2.9	3.9	10.6
836	7.8	10.4	14.4	39.2	2.6	3.6	9.7
980	8.5	8.9	13.0	35.0	2.2	3.2	8.7
		HeI (1s4p)$^1P^0$			HeI (1s5p)$^1P^0$		
35	1.6	2.54	0.58	3.71	–	–	–
65	2.2	5.17	1.52	8.23	–	–	–
80	2.4	5.69	2.13	9.95	3.21	1.19	5.59
150	3.3	4.45	2.73	9.90	2.53	1.54	5.61
200	3.8	3.64	2.66	8.96	2.07	1.51	5.10
276	4.5	2.82	2.45	7.72	1.62	1.39	4.40
340	5.0	2.36	2.27	6.91	1.36	1.29	3.94
412	5.5	1.99	2.09	6.17	1.13	1.19	3.51
500	6.1	1.66	1.90	5.47	0.94	1.08	3.10
575	6.5	1.46	1.77	5.00	0.83	1.00	2.83
667	7.0	1.27	1.63	4.52	0.72	0.92	2.57
735	7.3	1.16	1.54	4.23	0.66	0.87	2.40
836	7.8	1.02	1.42	3.87	0.58	0.81	2.19
980	8.5	0.88	1.29	3.45	0.50	0.73	1.96

Table 1C
Magnetic sublevel angle-integrated and total cross-sections for decay of He (1snp) $^1P^0$ ($n = 2$–5) states following electron and proton impact – C. Electron cross-sections: Born 1. See page 50 for Explanation of Tables

Energy (eV)	Velocity (a.u.)	HeI (1s2p) $^1P^0$			HeI (1s3p) $^1P^0$		
		$\bar{\sigma}_0$ (10^{-19}cm^2)	$\bar{\sigma}_1$ (10^{-19}cm^2)	$\bar{\sigma}$ (10^{-19}cm^2)	$\bar{\sigma}_0$ (10^{-19}cm^2)	$\bar{\sigma}_1$ (10^{-19}cm^2)	$\bar{\sigma}$ (10^{-19}cm^2)
80	2.4	75.79	32.60	140.99	18.965	7.786	34.536
150	3.3	47.26	31.26	109.78	11.764	7.614	26.992
200	3.8	37.03	28.66	94.34	9.193	7.007	23.207
276	4.5	27.82	25.16	78.15	6.892	6.169	19.229
340	5.0	23.00	22.80	68.60	5.690	5.595	16.881
412	5.5	19.25	20.65	60.54	4.757	5.071	14.898
500	6.1	16.05	18.55	53.15	3.963	4.559	13.080
575	6.5	14.06	17.10	48.27	3.470	4.205	11.879
667	7.0	12.21	15.64	43.49	3.011	3.846	10.704
735	7.3	11.13	14.73	40.59	2.744	3.622	9.988
836	7.8	9.84	13.57	36.99	2.424	3.339	9.102
980	8.5	8.45	12.24	32.93	2.079	3.012	8.102
		HeI (1s4p)$^1P^0$			HeI (1s5p)$^1P^0$		
80	2.4	8.001	3.285	14.570	4.096	1.682	7.460
150	3.3	4.963	3.212	11.387	2.541	1.645	5.830
200	3.8	3.878	2.956	9.790	1.986	1.513	5.013
276	4.5	2.907	2.602	8.112	1.489	1.332	4.153
340	5.0	2.401	2.361	7.122	1.229	1.209	3.646
412	5.5	2.007	2.139	6.285	1.028	1.095	3.218
500	6.1	1.672	1.923	5.518	0.856	0.985	2.825
575	6.5	1.464	1.774	5.011	0.750	0.908	2.566
667	7.0	1.270	1.623	4.516	0.650	0.831	2.312
735	7.3	1.157	1.528	4.214	0.593	0.782	2.157
836	7.8	1.023	1.409	3.840	0.524	0.721	1.966
980	8.5	0.877	1.270	3.418	0.449	0.650	1.750

Table 1D
Magnetic sublevel angle-integrated and total cross-sections for decay of He (1snp) $^1P^0$ ($n = 2$–5) states following electron and proton impact – D. Electron cross-sections: RMPS. See page 50 for Explanation of Tables

Energy (eV)	Velocity (a.u.)	HeI (1s2p) $^1P^0$		
		$\bar{\sigma}_0$ (10^{-19}cm^2)	$\bar{\sigma}_1$ (10^{-19}cm^2)	$\bar{\sigma}$ (10^{-19}cm^2)
30	1.5	21.43	5.45	32.34
60	2.1	53.15	17.46	88.08
80	2.4	54.73	22.47	99.67
150	3.3	42.49	26.12	94.74
200	3.8	34.68	25.65	85.98
276	4.5	26.65	23.13	72.91
340	5.0	22.01	21.28	64.58

Table 1E
Magnetic sublevel angle-integrated and total cross-sections for decay of He (1snp) $^1P^0$ ($n = 2$–5) states following electron and proton impact – E. Proton cross-sections: Experiment. See page 50 for Explanation of Tables

Energy (eV)	Velocity (a.u.)	HeI (1s2p) $^1P^0$			HeI (1s3p) $^1P^0$		
		$\bar{\sigma}_0$ (10^{-19}cm^2)	$\bar{\sigma}_1$ (10^{-19}cm^2)	$\bar{\sigma}$ (10^{-19}cm^2)	$\bar{\sigma}_0$ (10^{-19}cm^2)	$\bar{\sigma}_1$ (10^{-19}cm^2)	$\bar{\sigma}$ (10^{-19}cm^2)
50	1.4	32.3 ± 4.1	26.7 ± 3.4	85.8 ± 7.7	7.0 ± 0.9	5.8 ± 0.7	18.5 ± 1.7
100	2.0	66.9 ± 8.5	57.0 ± 7.3	181.0 ± 16.3	14.9 ± 1.9	12.7 ± 1.6	40.3 ± 3.6
156	2.5	44.2 ± 5.7	39.2 ± 5.0	122.5 ± 11.0	10.8 ± 1.4	9.5 ± 1.2	29.8 ± 2.7
225	3.0	40.1 ± 5.1	36.4 ± 4.7	112.8 ± 10.2	9.6 ± 1.2	8.7 ± 1.1	27.0 ± 2.4
307	3.5	30.8 ± 4.0	31.0 ± 4.0	92.7 ± 8.3	7.7 ± 1.0	7.7 ± 1.0	23.1 ± 2.1
368	3.8	28.2 ± 3.6	29.8 ± 3.8	87.7 ± 7.9	7.7 ± 1.0	8.2 ± 1.1	24.1 ± 2.2
400	4.0	25.6 ± 3.3	27.4 ± 3.5	80.4 ± 7.2	6.7 ± 0.9	7.1 ± 0.9	21.0 ± 1.9
626	5.0	19.2 ± 2.5	24.2 ± 3.1	67.6 ± 6.1	4.5 ± 0.6	5.6 ± 0.7	15.7 ± 1.4
916	6.1	11.7 ± 1.5	16.9 ± 2.2	45.6 ± 4.1	3.1 ± 0.4	4.6 ± 0.6	12.3 ± 1.1
1400	7.5	9.1 ± 1.1	14.4 ± 1.8	38.0 ± 3.4	2.5 ± 0.3	3.9 ± 0.5	10.4 ± 0.9
		HeI (1s4p)$^1P^0$			HeI (1s5p)$^1P^0$		
50	1.4	2.4 ± 0.4	2.0 ± 0.4	6.3 ± 0.8	1.4 ± 0.3	1.2 ± 0.3	3.7 ± 0.6
100	2.0	5.9 ± 1.1	5.0 ± 0.9	15.8 ± 2.1	3.2 ± 0.8	2.8 ± 0.7	8.7 ± 1.5
156	2.5	4.5 ± 0.8	4.0 ± 0.7	12.5 ± 1.6	2.5 ± 0.6	2.2 ± 0.5	6.9 ± 1.2
225	3.0	4.0 ± 0.8	3.7 ± 0.7	11.4 ± 1.5	2.1 ± 0.5	1.9 ± 0.5	6.0 ± 1.0
307	3.5	3.5 ± 0.7	3.5 ± 0.7	10.5 ± 1.4	1.9 ± 0.5	1.9 ± 0.5	5.8 ± 1.0
368	3.8	3.0 ± 0.6	3.1 ± 0.6	9.2 ± 1.2	1.6 ± 0.4	1.7 ± 0.4	5.0 ± 0.8
400	4.0	3.0 ± 0.6	3.2 ± 0.6	9.5 ± 1.2	1.5 ± 0.4	1.7 ± 0.4	4.9 ± 0.8
626	5.0	1.9 ± 0.4	2.4 ± 0.5	6.7 ± 0.9	1.1 ± 0.3	1.3 ± 0.3	3.8 ± 0.6
916	6.1	1.3 ± 0.2	1.9 ± 0.4	5.2 ± 0.7	0.7 ± 0.2	1.0 ± 0.2	2.6 ± 0.4
1400	7.5	1.1 ± 0.2	1.7 ± 0.3	4.4 ± 0.6	0.6 ± 0.1	0.9 ± 0.2	2.5 ± 0.4

Table 1F
Magnetic sublevel angle-integrated and total cross-sections for decay of He (1snp) $^1P^0$ ($n = 2$–5) states following electron and proton impact – F. Proton cross-sections: AOCC. See page 50 for Explanation of Tables

Energy (eV)	Velocity (a.u.)	HeI (1s2p) $^1P^0$			HeI (1s3p) $^1P^0$		
		$\bar{\sigma}_0$ (10^{-19}cm^2)	$\bar{\sigma}_1$ (10^{-19}cm^2)	$\bar{\sigma}$ (10^{-19}cm^2)	$\bar{\sigma}_0$ (10^{-19}cm^2)	$\bar{\sigma}_1$ (10^{-19}cm^2)	$\bar{\sigma}$ (10^{-19}cm^2)
50	1.4	33.9	29.5	92.8	7.8	7.8	23.4
100	2.0	66.0	44.9	155.9	18.2	12.4	43.0
156	2.5	57.5	43.1	143.6	15.1	11.7	38.4
225	3.0	47.7	37.7	123.1	11.5	9.6	30.8
307	3.5	38.9	34.1	107.0	9.4	8.6	26.6
368	3.8	34.0	31.7	97.3	8.2	7.9	24.1
400	4.0	31.2	31.1	93.3	8.1	8.1	24.3
626	5.0	21.7	24.3	70.2	5.3	6.0	17.3
916	6.1	15.0	19.3	53.7	3.7	4.8	13.2
1400	7.5	9.0	13.8	36.6	2.4	3.6	9.6
		HeI (1s4p)$^1P^0$			HeI (1s5p)$^1P^0$		
50	1.4	3.46	3.22	9.89	1.77	1.65	5.06
100	2.0	7.69	5.23	18.15	3.94	2.68	9.29
156	2.5	6.43	4.89	16.21	3.29	2.50	8.30
225	3.0	4.94	4.01	12.97	2.53	2.06	6.64
307	3.5	4.03	3.60	11.22	2.06	1.84	5.74
368	3.8	3.51	3.32	10.15	1.80	1.70	5.20
400	4.0	3.42	3.42	10.27	1.75	1.75	5.26
626	5.0	2.24	2.53	7.29	1.14	1.30	3.73
916	6.1	1.56	2.01	5.57	0.80	1.03	2.85
1400	7.5	1.00	1.51	4.03	0.51	0.78	2.06

Table 1G
Magnetic sublevel angle-integrated and total cross-sections for decay of He (1snp) $^1P^0$ ($n = 2$–5) states following electron and proton impact – G. Proton cross-sections: Born 1. See page 50 for Explanation of Tables

Energy (eV)	Velocity (a.u.)	HeI (1s2p) $^1P^0$			HeI (1s3p) $^1P^0$		
		$\bar{\sigma}_0$ (10^{-19}cm^2)	$\bar{\sigma}_1$ (10^{-19}cm^2)	$\bar{\sigma}$ (10^{-19}cm^2)	$\bar{\sigma}_0$ (10^{-19}cm^2)	$\bar{\sigma}_1$ (10^{-19}cm^2)	$\bar{\sigma}$ (10^{-19}cm^2)
50	1.4	110.400	45.715	201.83	27.502	11.148	49.798
100	2.0	83.503	46.948	177.40	20.740	11.571	43.882
156	2.5	63.876	43.171	150.22	15.795	10.658	37.111
225	3.0	49.369	38.515	126.40	12.173	9.509	31.191
307	3.5	38.885	34.060	107.00	9.573	8.406	26.385
368	3.8	33.597	31.403	96.40	8.266	7.749	23.763
400	4.0	31.365	30.187	91.74	7.715	7.448	22.610
626	5.0	21.391	23.922	69.23	5.257	5.899	17.054
916	6.1	15.234	19.177	53.59	3.741	4.727	13.196
1400	7.5	10.327	14.679	39.69	2.534	3.618	9.769
		HeI (1s4p)$^1P^0$			HeI (1s5p)$^1P^0$		
50	1.4	11.602	4.703	21.009	5.940	2.408	10.756
100	2.0	8.750	4.882	18.513	4.480	2.499	9.479
156	2.5	6.664	4.496	15.656	3.412	2.302	8.016
225	3.0	5.135	4.012	13.159	2.629	2.054	6.737
307	3.5	4.039	3.546	11.131	2.068	1.816	5.699
368	3.8	3.487	3.269	10.025	1.785	1.674	5.133
400	4.0	3.255	3.142	9.539	1.666	1.609	4.884
626	5.0	2.218	2.489	7.195	1.135	1.274	3.684
916	6.1	1.578	1.994	5.567	0.808	1.021	2.850
1400	7.5	1.069	1.526	4.121	0.547	0.781	2.110

Table 2A
Degree of linear polarization and cross-section ratio $\bar{\sigma}_0/\bar{\sigma}_1$ for decay of HeI (1s2p) $^1P^0$ states following electron and proton impact – A. Electron data. See page 50 for Explanation of Tables

Energy (eV)	Velocity (a.u.)	Experiment		CCC		Born 1		RMPS	
		P	$\bar{\sigma}_0/\bar{\sigma}_1$	P	$\bar{\sigma}_0/\bar{\sigma}_1$	P	$\bar{\sigma}_0/\bar{\sigma}_1$	P	$\bar{\sigma}_0/\bar{\sigma}_1$
30	1.5	0.52 ± 0.08	3.17 ± 2.20	–	–	–	–	0.594	3.930
35	1.6	–	–	0.635	4.48	–	–	0.608	4.104
60	2.1	0.52 ± 0.02	3.17 ± 0.55	–	–	–	–	0.505	3.044
65	2.2	–	–	0.475	2.81	–	–	0.476	2.818
80	2.4	0.43 ± 0.02	2.51 ± 0.30	0.412	2.40	0.398	2.325	0.418	2.436
150	3.3	0.23 ± 0.01	1.60 ± 0.05	0.221	1.57	0.204	1.512	0.239	1.627
200	3.8	0.16 ± 0.01	1.37 ± 0.04	0.142	1.33	0.127	1.292	0.150	1.352
276	4.5	0.08 ± 0.01	1.17 ± 0.03	0.061	1.13	0.050	1.105	0.071	1.152
340	5.0	0.02 ± 0.01	1.05 ± 0.02	0.011	1.02	0.004	1.009	0.017	1.034
412	5.5	-0.02 ± 0.01	0.96 ± 0.02	−0.031	0.94	−0.035	0.932	–	–
500	6.1	-0.05 ± 0.01	0.90 ± 0.02	−0.070	0.87	−0.072	0.865	–	–
575	6.5	-0.09 ± 0.01	0.84 ± 0.01	−0.097	0.82	−0.098	0.822	–	–
667	7.0	-0.11 ± 0.01	0.81 ± 0.01	−0.124	0.78	−0.123	0.781	–	–
735	7.3	-0.12 ± 0.01	0.79 ± 0.01	−0.141	0.75	−0.139	0.756	–	–
836	7.8	-0.13 ± 0.01	0.78 ± 0.01	−0.162	0.72	−0.159	0.725	–	–
980	8.5	-0.14 ± 0.01	0.76 ± 0.01	−0.188	0.68	−0.183	0.690	–	–

Table 2B
Degree of linear polarization and cross-section ratio $\bar{\sigma}_0/\bar{\sigma}_1$ for decay of HeI (1s2p) $^1P^0$ states following electron and proton impact – B. Proton data. See page 50 for Explanation of Tables

Energy (keV)	Velocity (a.u.)	Experiment		Born 1		AOCC	
		P	$\bar{\sigma}_0/\bar{\sigma}_1$	P	$\bar{\sigma}_0/\bar{\sigma}_1$	P	$\bar{\sigma}_0/\bar{\sigma}_1$
50	1.4	0.095 ± 0.010[a]	1.21 ± 0.03	0.414	2.42	0.068	1.15
100	2.0	0.080 ± 0.010[a]	1.17 ± 0.03	0.280	1.78	0.190	1.47
156	2.5	0.061 ± 0.010	1.13 ± 0.03	0.193	1.48	0.144	1.34
225	3.0	-0.048 ± 0.010	1.10 ± 0.02	0.124	1.28	0.117	1.26
307	3.5	-0.002 ± 0.010	1.00 ± 0.02	0.066	1.14	0.066	1.14
368	3.8	-0.027 ± 0.010	0.95 ± 0.02	0.034	1.07	0.036	1.08
400	4.0	-0.034 ± 0.010	0.93 ± 0.02	0.019	1.04	0.002	1.00
626	5.0	-0.116 ± 0.012	0.79 ± 0.02	−0.056	0.89	−0.057	0.89
916	6.1	-0.185 ± 0.014	0.69 ± 0.01	−0.115	0.79	−0.124	0.78
1400	7.5	-0.224 ± 0.020[a]	0.63 ± 0.02	−0.174	0.70	−0.209	0.65

[a] Experimental polarization values for 50, 100, and 1400 keV protons were extrapolated using a least squares fit.

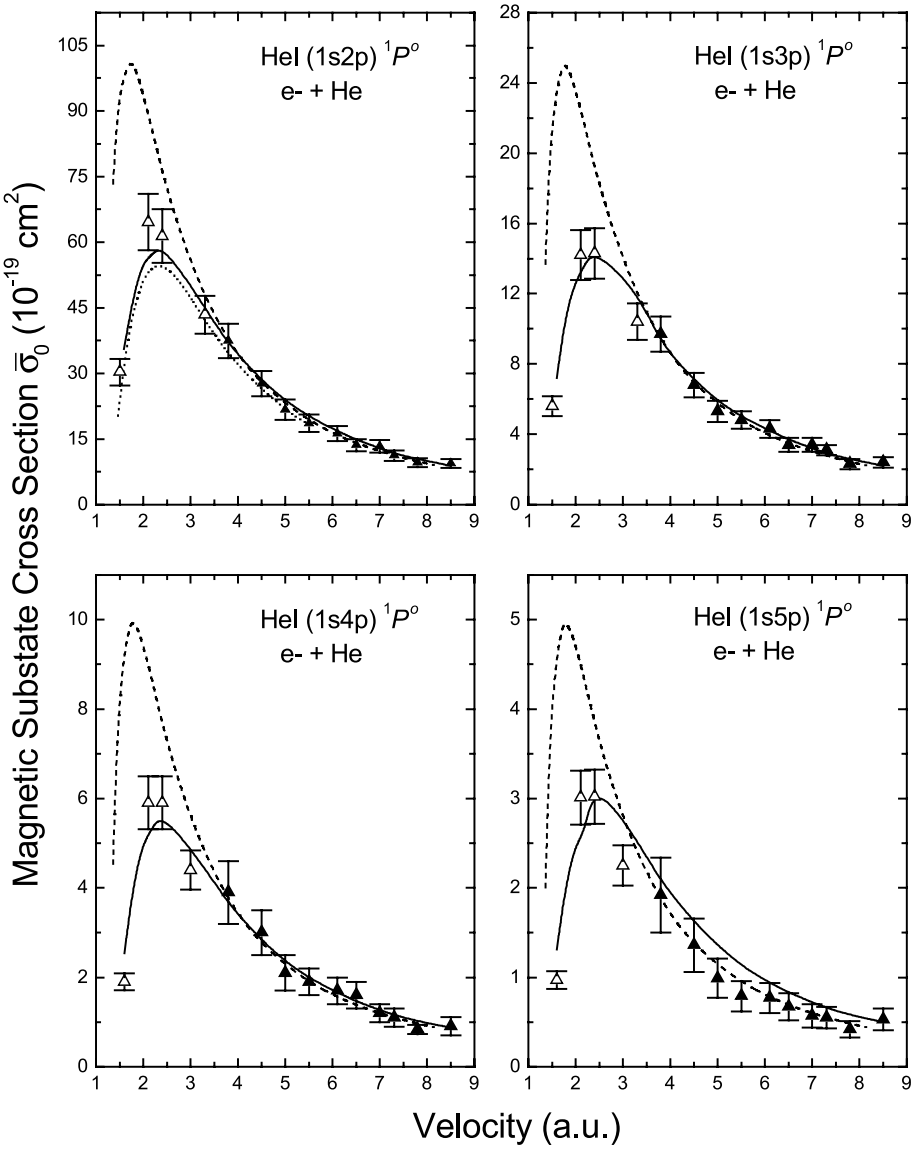

Fig. 1. Magnetic scattering angle-integrated substate cross-sections $\bar{\sigma}_0$. See page 51 for Explanation of Graphs.

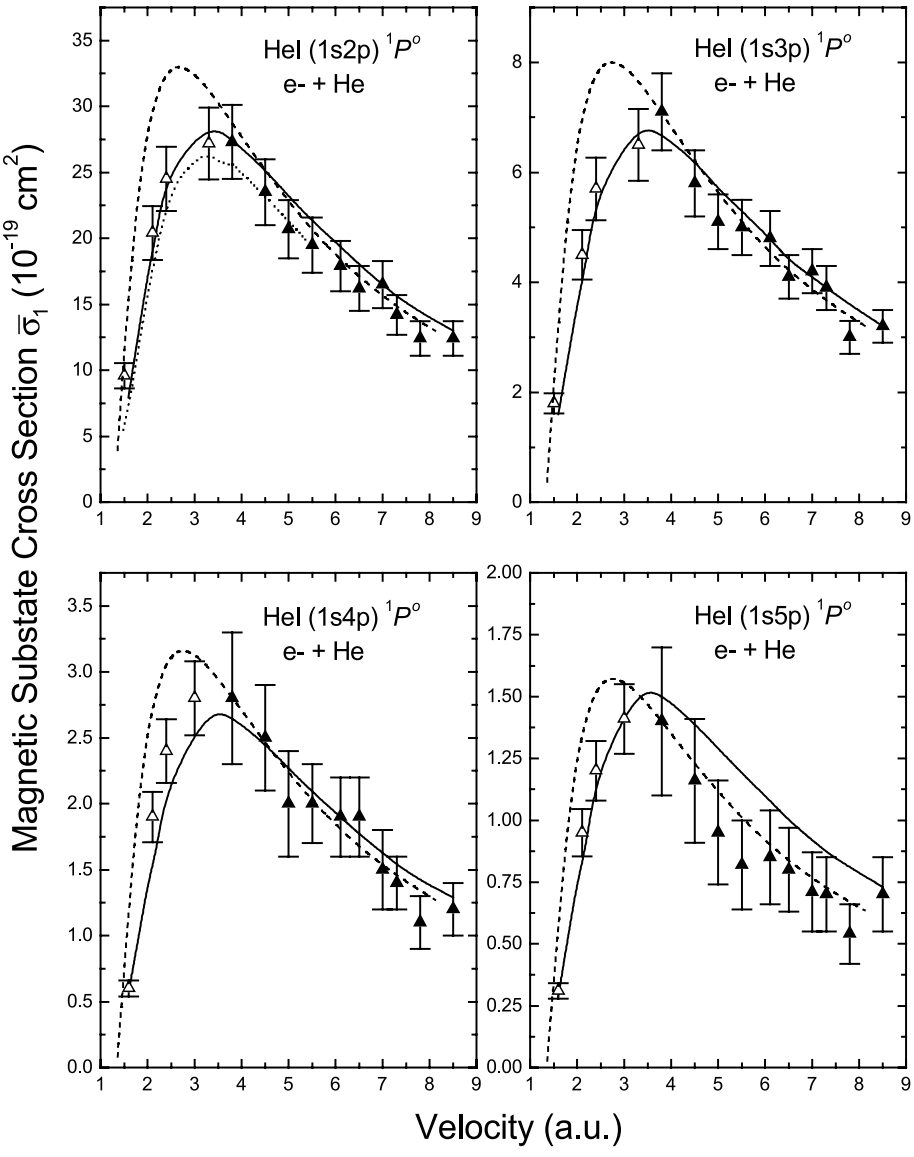

Fig. 2. Magnetic scattering angle-integrated substate cross-sections $\bar{\sigma}_1$. See page 51 for Explanation of Graphs.

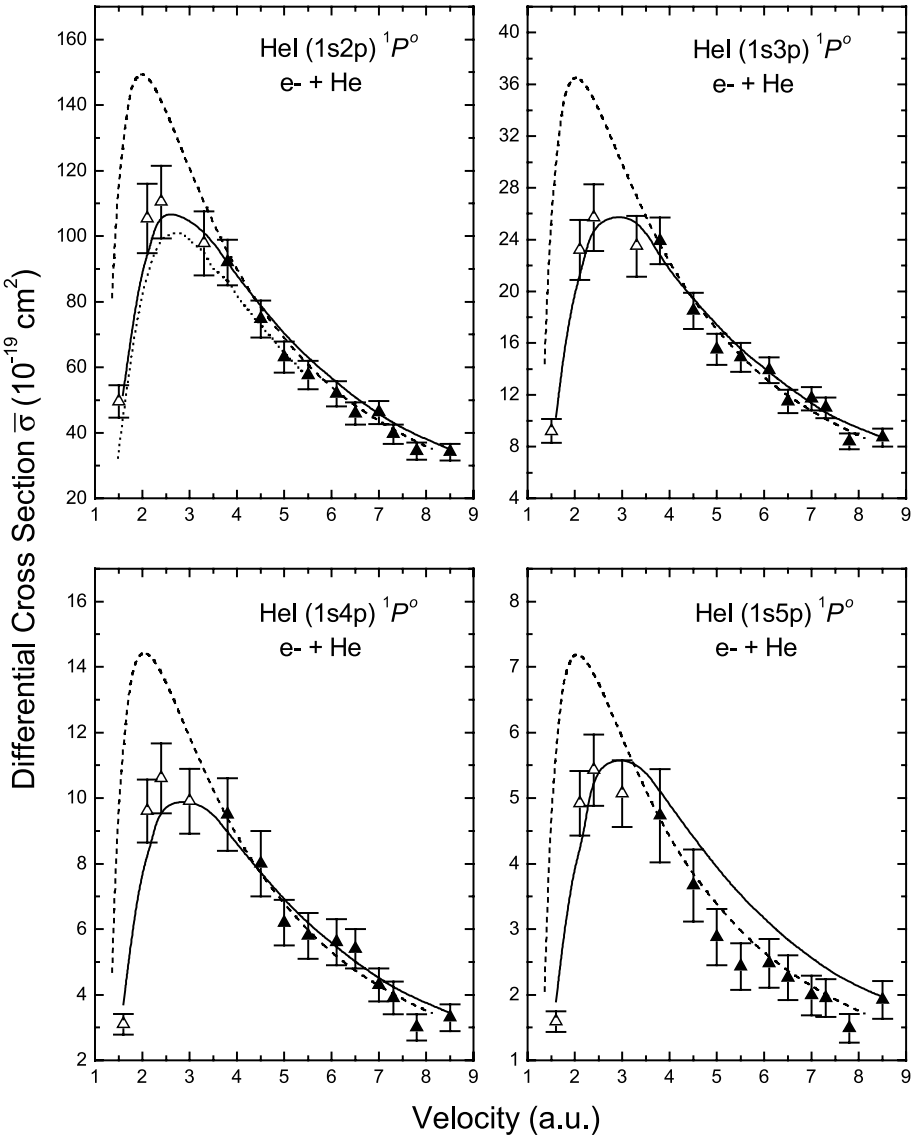

Fig. 3. Differential cross-sections $\bar{\sigma}$. See page 51 for Explanation of Graphs.

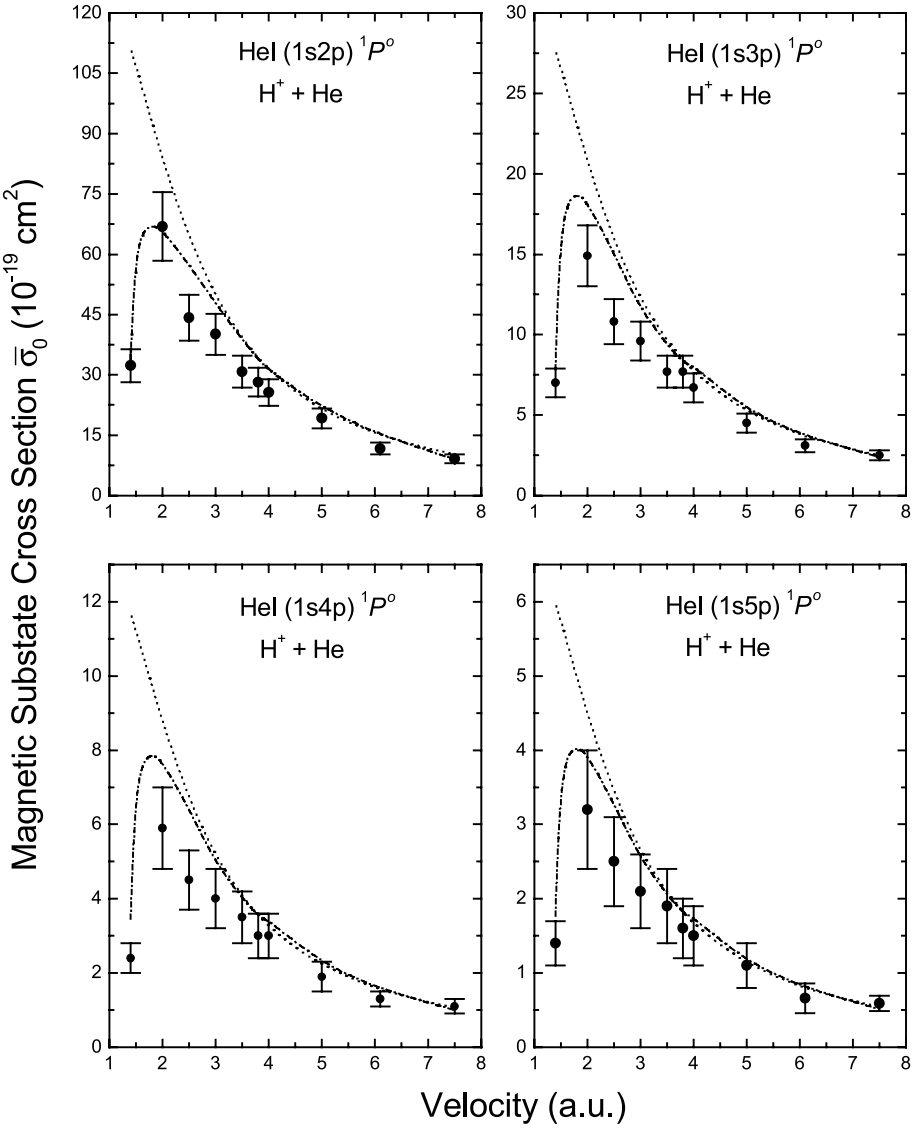

Fig. 4. Magnetic scattering angle-integrated substate cross-sections $\bar{\sigma}_0$. See page 51 for Explanation of Graphs.

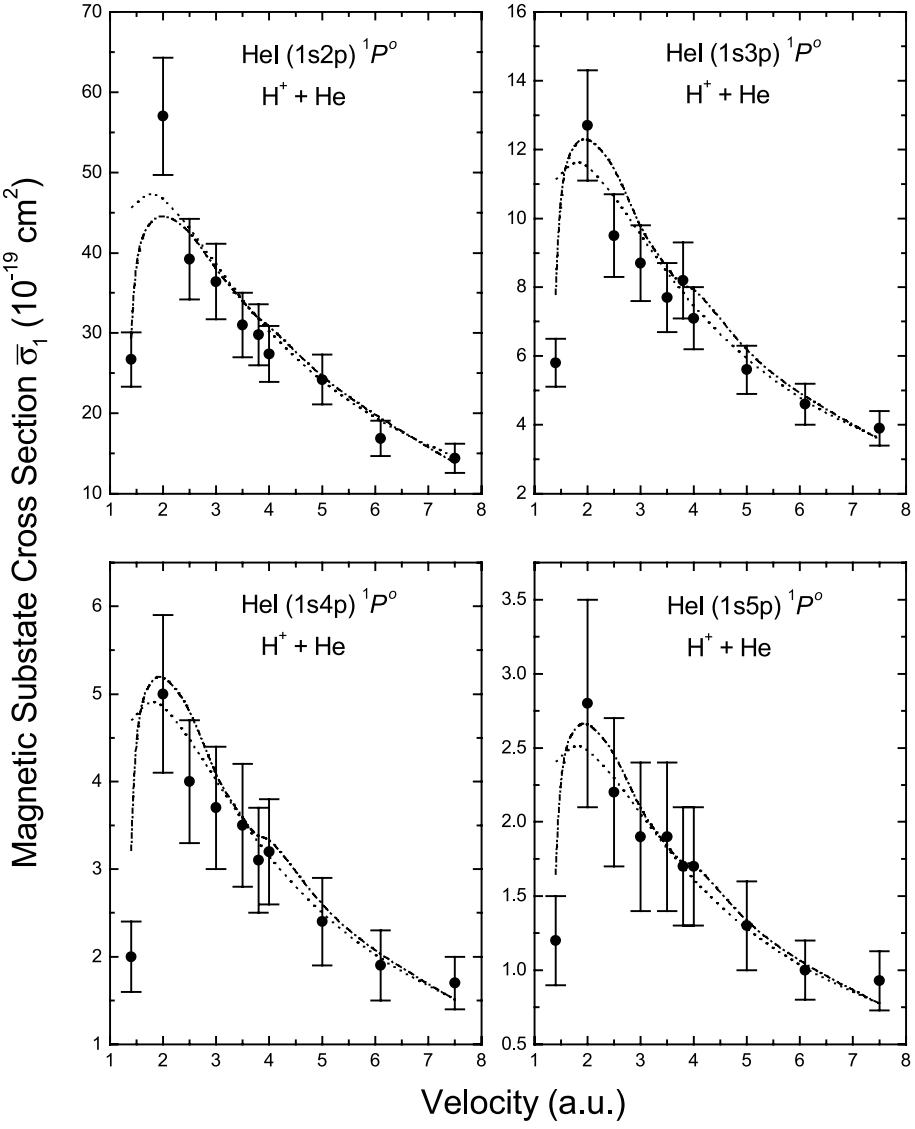

Fig. 5. Magnetic scattering angle-integrated substate cross-sections $\bar{\sigma}_1$. See page 51 for Explanation of Graphs.

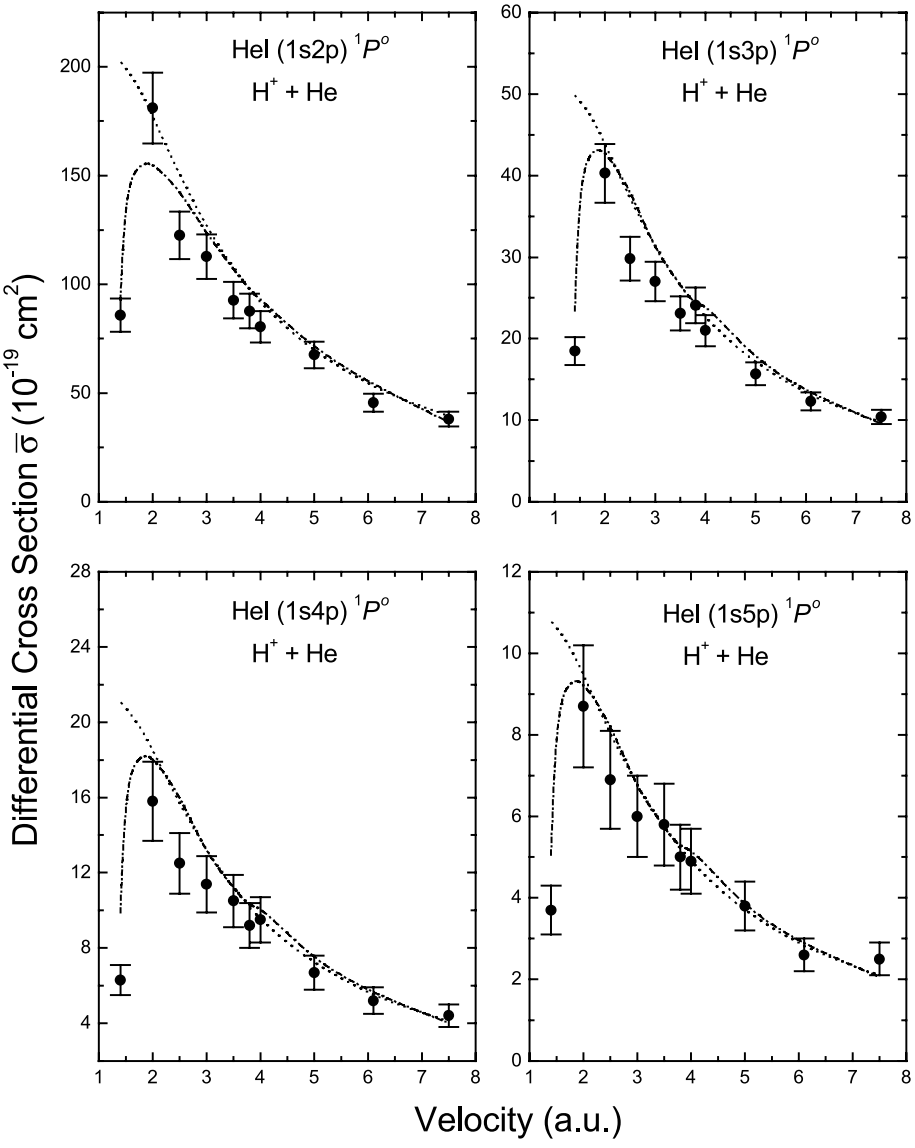

Fig. 6. Differential cross-sections $\bar{\sigma}$. See page 51 for Explanation of Graphs.

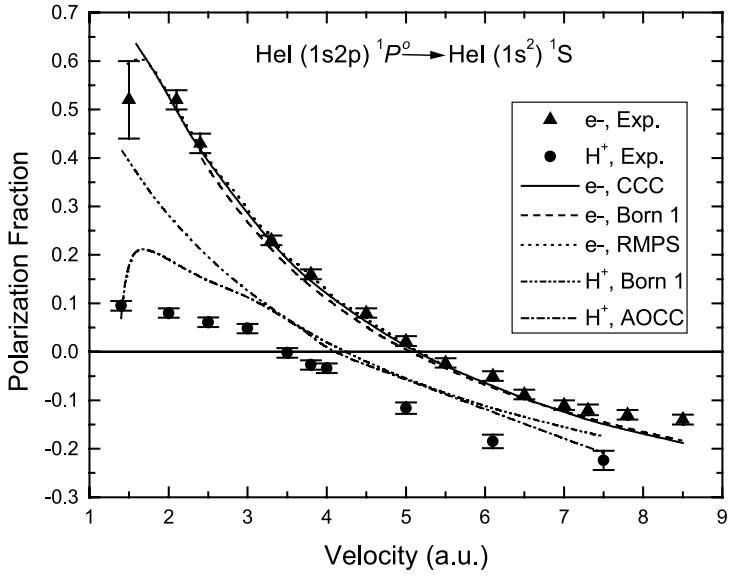

Fig. 7. Degree of linear polarization *P*. See page 51 for Explanation of Graphs.

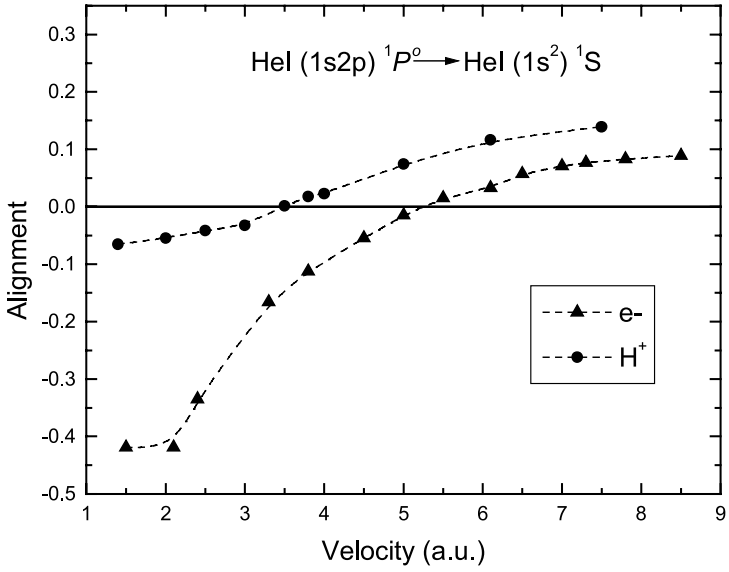

Fig. 8. Alignment A_0. See page 51 for Explanation of Graphs.

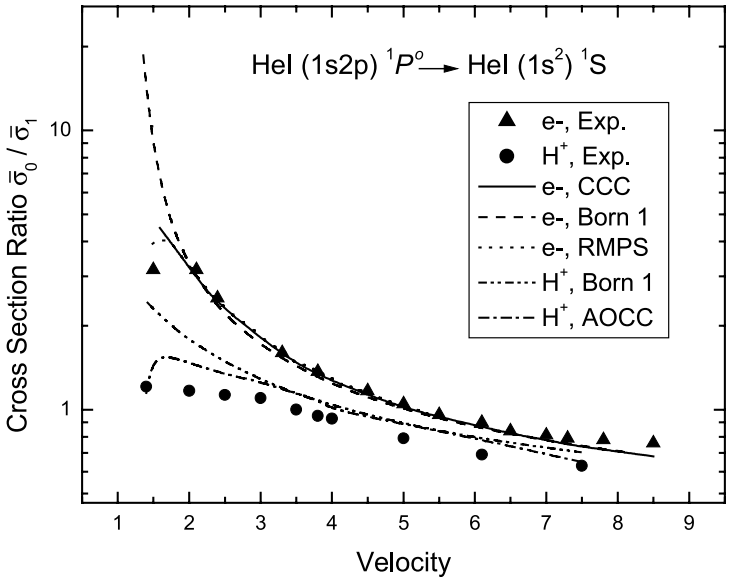

Fig. 9. Cross-section ratios $\bar{\sigma}_0/\bar{\sigma}_1$. See page 51 for Explanation of Graphs.